World Environmental and Water Resources Congress 2020

Groundwater, Sustainability, Hydro-Climate/Climate Change, and Environmental Engineering

Selected Papers from the Proceedings of the World Environmental and Water Resources Congress 2020

Henderson, Nevada • May 17–21, 2020

EDITED BY

Sajjad Ahmad, Ph.D.

Regan Murray, Ph.D.

ASCE

EWRI ASCE ENVIRONMENTAL & WATER RESOURCES INSTITUTE

WORLD ENVIRONMENTAL AND WATER RESOURCES CONGRESS 2020

GROUNDWATER, SUSTAINABILITY, HYDRO-CLIMATE/CLIMATE CHANGE, AND ENVIRONMENTAL ENGINEERING

SELECTED PAPERS FROM THE WORLD ENVIRONMENTAL AND WATER RESOURCES CONGRESS 2020

May 17–21, 2020
Henderson, Nevada

SPONSORED BY
Environmental and Water Resources Institute
of the American Society of Civil Engineers

EDITED BY
Sajjad Ahmad, Ph.D.
Regan Murray, Ph.D.

Published by the American Society of Civil Engineers

Published by American Society of Civil Engineers
1801 Alexander Bell Drive
Reston, Virginia, 20191-4382
www.asce.org/publications | ascelibrary.org

Errata: **Errata, if any, can be found at https://doi.org/10.1061/9780784482964**

ISBN 978-0-7844-8296-4 (PDF)
Manufactured in the United States of America.

Front cover: Photos courtesy of Sajjad Ahmad, Ph.D., P.E. Used with permission.

Numerical and Experimental Investigation of Active and Passive Spreading for Groundwater Remediation

R. M. Neupauer, Ph.D., P.E., M.ASCE[1]; L. J. Sather, Ph.D.[2]; E. J. Roth, Ph.D.[3]; D. C. Mays, Ph.D., P.E., M.ASCE[4]; and J. P. Crimaldi, Ph.D.[5]

[1]Dept. of Civil, Environmental, and Architectural Engineering, Univ. of Colorado Boulder, Boulder, CO. E-mail: neupauer@colorado.edu
[2]Wildermuth Environmental Inc., Lake Forest, CA. E-mail: lauren.reising@colorado.edu
[3]Dept. of Bioengineering, Univ. of Colorado Anschutz Medical Campus, Denver, CO. E-mail: eric.roth@colorado.edu
[4]Dept. of Civil Engineering, Univ. of Colorado Denver, Denver, CO. E-mail: david.mays@ucdenver.edu
[5]Dept. of Civil, Environmental, and Architectural Engineering, Univ. of Colorado Boulder, Boulder, CO. E-mail: crimaldi@colorado.edu

ABSTRACT

During in situ remediation of contaminated groundwater, a chemical or biological amendment is introduced into a contaminant plume to react with and degrade the contaminant. Since the degradation reactions only occur where the amendment and the contaminant are sufficiently close, the success of in situ remediation is controlled by the degree to which the amendment spreads into the contaminant plume. Spreading is defined as the reconfiguration of the plume geometry, which occurs as a result of spatially and temporally varying flow fields. Spreading can occur passively due to spatially varying velocity caused by aquifer heterogeneity. Spreading can also occur actively by inducing spatially and temporally varying flow fields through injections and extractions of clean water in wells surrounding the contaminated site. We used coupled numerical investigations and laboratory experiments to explore the effects of active spreading and passive spreading on contaminant degradation. We report here on the effects of passive spreading on contaminant degradation. We analyze the features of the flow field and plume geometry that encourage spreading contaminant degradation, so that the results from the numerical investigation and experiments can be used to design active spreading pumping sequences for other aquifers with other heterogeneity patterns.

INTRODUCTION

During in situ remediation of contaminated groundwater, a chemical amendment can be introduced into the contaminant plume to react with and degrade the contaminant. Degradation occurs where the contaminant and the amendment are sufficiently close so that mixing can bring them together to react. Mixing is the process that smooths concentration gradients through molecular diffusion and small-scale dispersion (Dentz et al., 2011). Mixing near the interface between the contaminant and amendment plumes (hereafter called the "plume interface") causes commingling of the plumes, allowing reaction to occur. Mixing is influenced by the complementary process of spreading, which reconfigures the plume geometry (Dentz et al., 2011). Spreading can lead to elongation of the plume interface, thereby increasing the surface along which mixing can occur. It can also lead to sharpening of the concentration gradient, thereby increasing diffusive and dispersive mass fluxes and the amount of mixing.

Spreading can occur both passively and actively. Passive spreading occurs when the plumes

travel through a heterogeneous aquifer. As the plumes flow preferentially toward higher permeability zones and preferentially away from lower permeability zones, the plume geometry changes. Active spreading occurs when injection and extraction wells are used to induce spatial, and possibly temporal, variations in velocity. As different parts of the plume travel at different velocities, the plume geometry changes. In general, during active and passive spreading, some parts of the plume interface are stretched, while other parts contract. With a thorough understanding of the behaviors that lead to stretching and contraction and knowledge of the local heterogeneity, one can design a remediation system to create an active spreading scenario that complements the passive spreading created by the heterogeneity to achieve a high amount of contaminant degradation.

To evaluate the combined effects of active and passive spreading on contaminant degradation, we performed numerical simulations of reactive transport for a suite of active spreading scenarios and heterogeneity patterns (Reising, 2018). Before we can interpret the coupled effects of active spreading and passive spreading on reaction, we consider first the individual effects of active spreading alone and of passive spreading alone on transport of a non-reactive solute. To analyze the effects of active spreading alone, we conducted experiments to investigate the movement of a conservative solute in an approximately homogeneous porous medium (i.e., no passive spreading) under multiple active spreading scenarios (Roth et al, in review). To analyze the effects of passive spreading alone, we performed a theoretical investigation of the effect of inhomogeneous inclusions on the transport of a conservative solute in an otherwise uniform flow. The results of the investigation on passive spreading are reported in this paper.

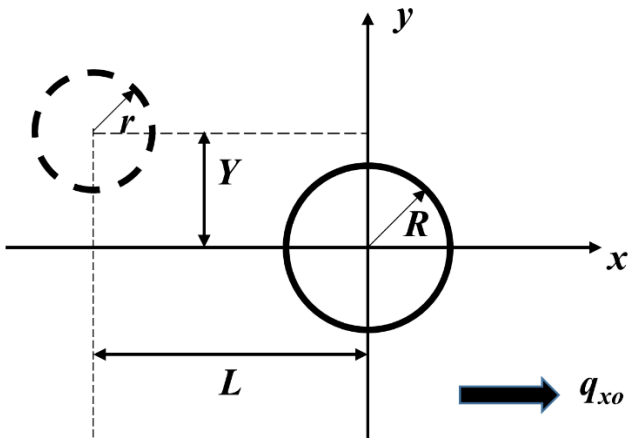

Figure 1. Plan view of aquifer. The circle with the solid outline represents the inclusion of radius *R*. The circle of radius *r* with the dashed outline represents the initial position of the solute plume. The center of the solute plume is offset from the center of the inclusion by distances of *L* and *Y* in the *x*- and *y*-directions, respectively. The thick arrow shows the direction of the far field flow.

THEORY

Groundwater Flow Theory: We consider a two-dimensional, isotropic, confined aquifer of infinite extent that is homogeneous except of a circular inclusion of radius R centered at the origin (see Figure 1). Using potential flow theory (e.g., Bear, 1972), the complex potential for

this aquifer is (Strack and Haitjema, 1981)

$$\Phi(z)=\begin{cases} q_{xo}\dfrac{2K_I z}{K+K_I}-K_I h_o & |z|\le R \\ q_{xo}\left[z+\dfrac{K-K_I}{K+K_I}\dfrac{R^2}{z}\right]-Kh_o & \text{otherwise}\end{cases} \tag{1}$$

where $z = x + iy$ is the complex coordinate, q_{xo} is the far field specific discharge, K and K_I are the hydraulic conductivities of the main aquifer and the inclusion, respectively, and h_o is the head at $x = 0$. From potential flow theory, the streamlines are defined by the imaginary part of the complex potential in (1), given by

$$\psi(x,y)=\begin{cases} q_{xo}\dfrac{2K_I y}{K+K_I} & |z|\le R \\ q_{xo}y\left[1-\dfrac{K-K_I}{K+K_I}\dfrac{R^2}{z^2}\right] & \text{otherwise}\end{cases} \tag{2}$$

where $\psi(x,y)$ is the stream function. Also, the specific discharge is the gradient of the real part of the complex potential in (1), given by

$$q_x(x,y)=\begin{cases} q_{xo}\dfrac{2K_I}{K+K_I} & |z|\le R \\ q_{xo}\left[1+\dfrac{K-K_I}{K+K_I}\dfrac{R^2}{z^2}\left(1-\dfrac{2x^2}{z^2}\right)\right] & \text{otherwise}\end{cases} \tag{3}$$

and

$$q_y(x,y)=\begin{cases} 0 & |z|\le R \\ q_{xo}\dfrac{K-K_I}{K+K_I}\dfrac{2xyR^2}{z^4} & \text{otherwise}\end{cases} \tag{4}$$

where q_x and q_y are the components of specific discharge in the x- and y-directions, respectively.

Solute Transport Theory: To illustrate the effects of active spreading alone, we consider advective transport only. The initial solute distribution is a circular plume of radius r, with its center at $(x,y) = (-L,Y)$ (see Figure 1). The initial solute distribution is

$$C(x,y)=\begin{cases} \dfrac{C_{\max}}{r}\left[r-\sqrt{(x+L)^2+(y-Y)^2}\right] & (x+L)^2+(y-Y)^2\le r^2 \\ 0 & \text{otherwise}\end{cases} \tag{5}$$

where $C_{\max}$ is the maximum concentration, which occurs at the plume center, and concentration decreases linearly with radial distance from the plume center. With this expression, the magnitude of concentration gradient in the radial direction in the interior of the plume is $C_{\max}/r$, except at the center where the gradient is undefined.

We can track the plume movement by tracking the movement of a small plume parcel along a streamline defined in (2). The travel time, T, across N segments of the streamline is given by

$$T=n\sum_{i=1}^{N}\frac{\Delta s_i}{|q_i|} \tag{6}$$

where n is porosity, Δs_i is the length of segment i, and $|q_i|$ is the magnitude of the specific discharge vector (calculated using components in (3) and (4)) at the upstream point of segment i.

We use (6) to find the position of each plume parcel at time T.

Spreading and Mixing Theory: During in situ remediation, reaction occurs as the amendment and contaminant are brought together by dispersion across the plume interface. Assuming instantaneous reaction and complete mixing in the pore space, the instantaneous reaction rate, $\dot{M}$, is therefore the magnitude of the instantaneous dispersive mass flow rate across the entire plume interface, given by (Reising, 2018)

$$\dot{M} = nb \oint_{\Gamma} D_{\beta} \left| \frac{\partial C}{\partial \beta} \right| d\Gamma \tag{7}$$

where Γ represents the plume interface, β is the direction locally perpendicular to the plume interface, D_β is the dispersion coefficient in the β direction perpendicular to the local plume interface, and $\left|\partial C/\partial \beta\right|$ is the magnitude of the gradient of the contaminant concentration in the β direction. Reising (2018) developed an expression for the dispersion coefficient, given by

$$D_{\beta} = |v| \left(\alpha_L \sin^2 \theta + \alpha_T \cos^2 \theta \right) \tag{8}$$

where $|v|$ is the magnitude of the local velocity vector, θ is the angle between the local velocity vector and the local tangent to the plume interface, and α_L and α_T are the longitudinal and transverse dispersivities, respectively. Since α_L and α_T differ by about an order of magnitude, while the velocity along the plume interface may differ by many orders of magnitude as parts of the plume pass through the inclusion, we assume that $\alpha_L = \alpha_T = \alpha$. Using this simplification in (8) and the fact that $q = v\, n$, (7) is simplified to

$$\dot{M} = \alpha b \oint_{\Gamma} |q| \left| \frac{\partial C}{\partial \beta} \right| d\Gamma \tag{9}$$

Thus, if spreading leads to an elongation of the interface, the integral in (9) is evaluated over a long contour, leading to more mixing and reaction. Also, if spreading sharpens in the concentration gradient in area of high specific discharge, the integrand in (9) increases, leading to more mixing and reaction.

In this work, we evaluate the effect of passive spreading on the potential for reaction by letting Γ in (9) represent the boundary of the plume of a conservative solute. We let α and b be constants, and for convenience, we set their product to a magnitude of unity. We calculate the magnitude of the gradient numerically by tracking the movement of 1000 uniformly spaced particles on the $C = 0$ and $C = aC_{\max}$ contours of the initial contaminant plume for a duration of time T. Then for each particle on the $C = 0$ contour of the final plume (at time T), we find the closest point on the $C = aC_{\max}$ contour of the final plume, and use that as the separation distance, d. Then we approximate the magnitude of the concentration gradient at that point as

$$\left| \frac{\partial C}{\partial \beta} \right| \approx \frac{aC_{\max}}{d} \tag{10}$$

We use numerical integration to evaluate the contour integral in (9).

RESULTS

We performed the analysis for the combinations of r, Y, and K_I shown in Table 1, with $K = 1$ m/d, $T = 15$ d, $q_{xo} = 0.05$ m/d, $R = 1$ m, $C_{\max} = 1$ g/m^3, $a = 0.15$, $L/R = 2.5$, and $n = 0.25$. The values of the plume boundary length and instantaneous reaction rate from (9) are also shown in Table 1 for each case. Some case are shown more than once, for ease of comparison. The initial and final plume positions and the streamlines are shown in Figures 2 and 3.

The results show that passive spreading leads to the most stretching (elongation of the plume boundary) for flow around a low-conductivity inclusion (Figure 2a,c,f). Less stretching occurs for flow through a high conductivity inclusion (Figure 2b,e,g); and no stretching occurs in a homogeneous aquifer (Figure 2d). If the plume size is equal to the size of the inclusion (first three rows in Table 1, Figure 2c-e), the change in the instantaneous reaction rate, $\dot{M}$, due to passive spreading is proportional to the elongation of the plume.

For the scenarios with the low conductivity inclusion, the plume stretching and instantaneous reaction rate increase as the size of the plume decreases (second set of three rows in Table 1, Figure 2a,c,f). In all cases the plume is folded around the inclusion. Due to the size of the smaller plume, the folded plume is much narrower in the direction perpendicular to the inclusion boundary, indicating that the concentration gradient is steeper, which leads to a higher instantaneous reaction rate. For scenarios with the high conductivity inclusion (third set of three rows in Table 1, Figure 2b,e,g), the stretching and instantaneous reaction rate increase as the size of the plume increases. This pattern occurs because the small plume remains on relatively horizontal streamlines, indicating that all parts of the plume move at similar velocities and in the same direction. On the other hand, the larger plume extends across curving streamlines, some of which bypass the inclusion; therefore, different portions of the plume travel at different velocities, leading to more stretching.

Table 1. Plume boundary length and instantaneous reaction rate, $\dot{M}$, for initial and final plumes for various combinations of r, Y, and K_I. The "Ratio" is the ratio of final value to initial value.

				Length of Γ (m)			$\dot{M}$ from (9) (mg/d)		
r/R	Y/R	K_I/K	subplot	Initial	Final	Ratio	Initial	Final	Ratio
1	0	0.1	2c	6.28	14.9	2.37	0.30	1.93	6.36
1	0	1	2d	6.28	6.28	1.00	0.31	0.31	1.00
1	0	10	2e	6.28	6.53	1.04	0.38	0.44	1.15
0.5	0	0.1	2a	3.14	11.3	3.59	0.28	15.2	53.9
1	0	0.1	2c	6.28	14.9	2.37	0.30	1.93	6.36
1.5	0	0.1	2f	9.42	18.1	1.92	0.33	1.05	3.19
0.5	0	10	2b	3.14	3.19	1.01	0.36	0.39	1.08
1	0	10	2e	6.28	6.53	1.04	0.38	0.44	1.15
1.5	0	10	2g	9.42	10.1	1.07	0.40	0.53	1.33
1	0	0.1	3a	6.28	14.9	2.37	0.30	1.93	6.36
1	0.5	0.1	3d	6.28	14.4	2.30	0.31	2.78	8.89
1	1	0.1	3f	6.28	9.18	1.46	0.34	0.50	1.48
1	0	10	3c	6.28	6.53	1.04	0.38	0.44	1.15
1	0.5	10	3e	6.28	6.59	1.05	0.38	0.48	1.27
1	1	10	3g	6.28	9.17	1.46	0.38	13.4	34.9

When the plume is offset from the inclusion (Figure 3), the effects depend on whether the inclusion has lower or higher hydraulic conductivity relative to the main aquifer. For a low conductivity inclusion with no offset, the plume folds around the inclusion (Figure 3a), leading to two narrow branches – one above the inclusion ($y > 0$) and one below the inclusion ($y < 0$). As the offset increases, the folded branch below the inclusion shrinks and the folded branch above the inclusion grows (Figure 3d,f) leading to a shorter plume boundary and shallower gradient.

The overall effect is that as the offset increases, the elongation of the plume boundary and the instantaneous reaction rate both decrease (fourth set of three rows in Table 1).

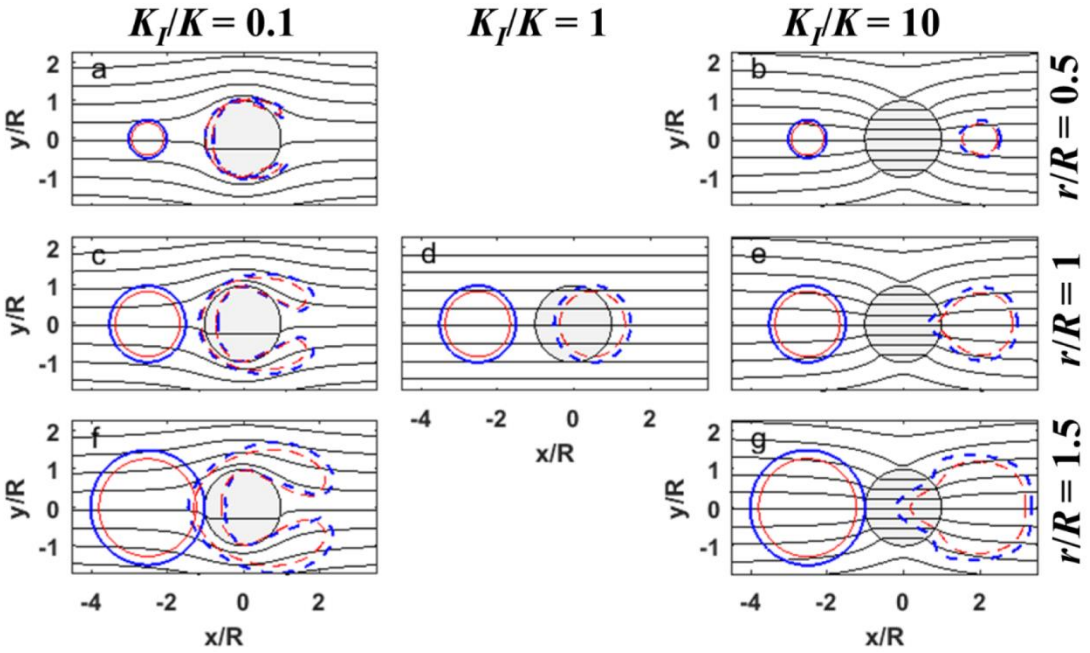

Figure 2. Initial (solid blue) and final (dashed blue) plume configurations for different combinations of K_I/K and r/R. The gray shaded area is the inclusion; the black lines are streamlines, and the red curves represent the initial (solid) and final (dashed) contours of aC_{max} used in the estimation of the concentration gradient.

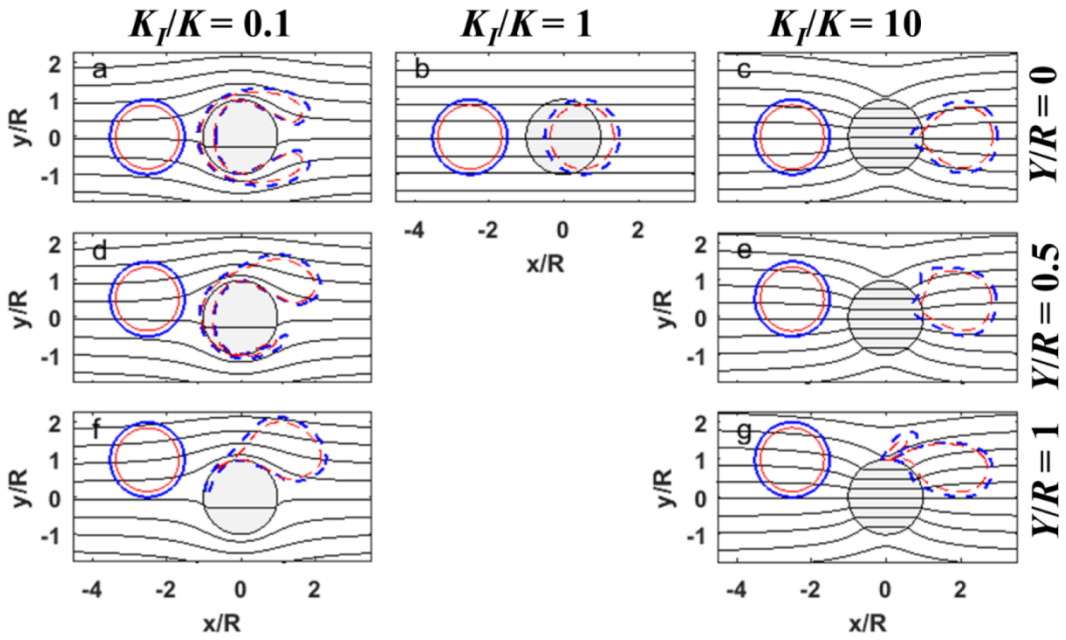

Figure 3. Initial (solid blue) and final (dashed blue) plume configurations for different combinations of K_I/K and Y/R. The gray shaded area is the inclusion; the black lines are streamlines, and the red curves represent the initial (solid) and final (dashed) contours of aC_{max} used in the estimation of the concentration gradient.

On the other hand, for a high conductivity inclusion (last set of rows lines in Table 1, Figure 3c,e,g), the elongation of the plume boundary and the instantaneous reaction rate increase slightly as the offset increases. This behavior occurs because, for the offsets evaluated here, increasing the offset leads to larger portions of the plume bypassing the inclusion, leading to different velocities for different portions of the plume, and ultimately more spreading.

CONCLUSION

The results of this study show that all passive spreading caused by an isolated inclusion increases the amount of plume spreading and reaction relative to a homogeneous aquifer. Thus, if a contaminated aquifer is poorly characterized, a remediation system designed under the assumption of a homogeneous aquifer to promote mixing-controlled reaction is likely to perform better than expected due to passive spreading caused by the inherent heterogeneity.

The results of this study also show that the hydraulic conductivity of an inclusion affects spreading and reaction. For low conductivity inclusions, the highest degree of spreading occurs if the plume is directed toward the inclusion in such a manner that the plume folds symmetrically around the inclusion, particularly if the inclusion is large relative to the size of the plume. Lower degrees of spreading are observed for high conductivity inclusions. Nevertheless, with a high conductivity inclusion, spreading is increased if the plume is directed to partially bypass the inclusion rather than passing directly through the inclusion. These results can provide guidance for the design of active spreading scenarios for in situ remediation if the heterogeneity of the site is well characterized.

ACKNOWLEDGMENT

This work was funded by the National Science Foundation under grants EAR-1417005 and EAR-1417017.

REFERENCES

Bear, J., *Dynamics of Fluids in Porous Media*, Dover Publications, Inc., New York, 1972.

Dentz, M. T. Le Borgne, A. Englert, and B. Bijeljic, Mixing, spreading, and reaction in heterogeneous media: A brief review. *J. Contam. Hydrol.*, *120-21*, 1-17, doi: 10.1016/j.jconhyd.2010.05.002, 2005.

Reising, L.J., *Numerical Investigations of Active and Passive Spreading to Enhance Mixing and Reaction in Porous Media*, Ph.D. dissertation, University of Colorado Boulder, Boulder, Colorado, 2018.

Roth, E.J., D.C. Mays, R.M. Neupauer, L.J. Sather, and J.P. Crimaldi, Methods for laser-induced fluorescence imaging of solute plumes in quasi-two-dimensional, refractive index-matched porous media, *Experiments in Fluids*, in review.

Strack, O.D.L. and H.M. Haitjema, Modeling double aquifer flow using a comprehensive potential and distributed singularities, 2, Solution for inhomogeneous permeabilities, *Water Resour. Res., 17*(5), 1551-1560, 1981.